Results in Engineering 27 (2025) 105723

Contents lists available at ScienceDirect

Results in Engineering

journal homepage: www.sciencedirect.com/journal/results-in-engineering

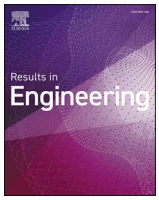

Research paper

Pinching simulation of the coconut crab considering the 3D shape and internal characteristics of the robust claw exoskeleton

Tadanobu Inoue [a,*], Michinori Iwai [b]

[a] National Institute for Materials Science, 1-2-1, Sengen, Tsukuba, Ibaraki 305-0047, Japan
[b] Japan Testing Laboratories, Inc., 1-71 Uchiwara, Ohgaki, Gifu 503-0936, Japan

ARTICLE INFO

Keywords:
Decapod crustacean
Claw
Finite element analysis (FEA)
X-ray CT
Biomechanics

ABSTRACT

A pinching simulation of the coconut crab, *Birgus latro*, which has a pinching force 80 times its body mass, was performed to quantify the stress imposed on the claw fingers when such a large force is applied. Data on the three-dimensional (3D) shape and internal information (hard exocuticle layer and soft endocuticle layer) in the claw exoskeleton were obtained using microfocus X-ray computed tomography. From these data, a 3D model of the claw was reconstructed using image analysis software, and a pinching simulation was performed using finite element analysis. The pinching force (R_f) was calculated as the sum of the node reaction forces in the area that came into contact with the stainless rod while the movable finger rotated within the claw, and the von Mises stress, σ_{mises}, in the fixed and movable fingers during the rotation were shown. The results showed that the stress increased with the angle of rotation, and at an angle of rotation of 2.8° and a reaction force of 957 N, stresses of 1.8 GPa were generated in the fixed finger, 588 MPa in the movable finger, and 674 MPa in the rod. This scientific pinching simulation confirmed the exceptional strength of the coconut crab's claw.

1. Introduction

Interest in the study of biological materials is growing because the understanding of biological mechanisms and their application leads to the development of new materials and technologies, driving innovation in various industries [1–6].

In general, the maximum force (F) exerted by animals flying, swimming, running, jumping, biting, or pinching has a positive correlation with their body mass (BW). Simply put, the biting force of a large-bodied lion or crocodile is greater than the pinching force of a small-bodied crab. However, when we divide this force by body mass and organize it into the force per unit mass (F/BW), the F/BW has a negative correlation with body mass. It has been suggested that most animals range between 0.5 $BW^{-1/3}$ and 20 $BW^{-1/3}$, but decapod crustaceans exceed that range [7,8]. Fig. 1 plots data from Huber et al. [9] and Oka et al. [10]. The pinching force relative to their body mass exerted by decapod crustaceans is stronger than that of other animals [8]. Against this backdrop, the previous studies mainly focused on the exoskeletons of the powerful crab claw, while the tissue structure [11–14], elemental composition [12,14,15], mechanical properties [13,15–19], and surface morphology [20,21] were clarified using advanced analytical approaches, such as scanning electron microscopy (SEM), energy-dispersive X-ray spectroscopy (EDS), X-ray diffraction (XRD), laser microscopy, and nanoindentation. Among crustaceans, the pinching force of the coconut crab, *Birgus latro*, which is the largest terrestrial crustacean, exceeds 80 times its BW [10,14]. However, little is known about the stress imposed on the claw fingers when such a strong force is applied.

The exoskeleton of the coconut crab is composed of the epicuticle (outermost surface wax layer), the exocuticle (hardest layer), the endocuticle (thickest layer), and the membranous layers (adjacent to the soft tissues) [14,15]. Two layers of the mineralized exocuticle and endocuticle are mineralized with calcite [22]; however, the mechanical properties vary significantly depending on the microstructure and calcium (Ca) concentration [16]. The exocuticle was five times harder than the endocuticle. The hard exocuticle—with a 28–33wt % Ca—has a twisted plywood structure stacked parallel to the surface, and the soft endocuticle—with a 20–25wt % Ca—has a porous structure with many regularly arranged pores normal to the surface [14–16]. By utilizing micro X-ray computed tomography (CT) scanning technology, we can obtain this internal information, including the external shape, without physically destroying the claw. From these data, a 3D model of the claws

* Corresponding author at: National Institute for Materials Science, 1-2-1, Sengen, Tsukuba 305-0047, Japan.
E-mail address: INOUE.Tadanobu@nims.go.jp (T. Inoue).

https://doi.org/10.1016/j.rineng.2025.105723
Received 23 April 2025; Received in revised form 4 June 2025; Accepted 10 June 2025
Available online 11 June 2025

can be reconstructed using image analysis software, and a pinching simulation using the finite element method should be possible. Yang et al. [23] investigated the mechanism of cavitation generated by snapping shrimps and the characteristics of the snapper claw motion through fluid dynamic simulation. To achieve this, a model equivalent to the snapper claw was constructed by CT scanning technology, and the production of cavitation bubbles by snapping shrimp was simulated. Sayekti et al. [24] studied the relationship between von Mises stress and crab carapace morphologies in relation to their impact properties using 3D scanning technology and finite element analysis. Neither study accounts for the internal information of the exoskeleton such as the exo- and endocuticle layers; however, by combining CT scanning technology and numerical analysis, simulations have been carried out that reflect the 3D shape of the crab in the model.

In this paper, we focused on the force acting on the robust claws of the coconut crab, which has a pinching force of 80 times its body mass. First, data on the three-dimensional (3D) shape and internal information (hard and soft layers) in the exoskeleton of the claw of the coconut crab were obtained using microfocus X-ray computed tomography (X-CT). A 3D model of the coconut crab's claw was then reconstructed and a pinching simulation was performed using finite element analysis (FEA). We attempted to quantify the stress generated at the contact area of the claw fingers when a coconut crab pinches a stainless steel rod, as was done in the pinching experiment shown in the previous paper [10].

2. Materials and methods

2.1. Sample preparation

A wild male coconut crab was captured at Motobu Town on northern Okinawa, Japan. The *BW* of the crab was 1290 g, and the thoracic length (*ThL*) was 56.1 mm. Based on *ThL*, this crab was estimated to be an adult 17–19 years old [25]. The pinching force (P_f) of the crab was estimated to be 957 N from the correlation between the P_f and *BW* [10]. In order to protect the wild coconut crabs inhabiting this area, we collected only the left claw for the sample. The crab was then released to the capture point. The claw length and height were 91 mm and 56 mm, respectively, as shown in Fig. 2(a,b). The sample was stored frozen at −18 °C to prevent the natural decay processes.

2.2. Microfocus X-ray CT scanning

The claw was thawed under running water, its movable finger was fixed in an open position, and the whole claw was scanned using a microfocus X-ray CT (XT H 320; Nikon Solutions Co., Ltd., Tokyo, Japan). A resolution scan with a pixel size of 48 μm was carried out at 120 kV and 130 μA, and 1800 projections were acquired over an angular range of 360° 3D and cross-sectional images were obtained with VGSTUDIO MAX ver. 2024.1 software (Volume Graphics Co., Ltd., Nagoya, Japan), as shown in Fig. 2(c–f). In a tomographic image of the exoskeleton, the regions of the exocuticle and denticle are shown in white, reflecting a high Ca concentration; gray indicates the endocuticle with a lower Ca concentration. The non-calcified small, black protrusions on the exoskeleton surface [22,26]; the soft tissues inside the claw; and the pore canal tube (pct) ⊥ surface [14,26] are shown in black, including the air.

2.3. Creation of a finite element model

Inside the crab exoskeleton, the mechanical properties change gradually or abruptly due to differences in the degree of mineralization and microstructure [12–17,20–22,26]. In addition, there are relatively thick tubules perpendicular to the surface (pct ⊥ surface) and many pores. On the exoskeleton surface, there are small non-calcified protrusions and setae. Their presence is clearly shown as the black areas in Fig. 2. Furthermore, in the joint-like area where the movable finger connects with the claw, there is a gel-like substance with excellent contractility. This is the arthrodial membrane, which consists of non-mineralized cuticle. It is extremely difficult to reflect all of this information in current finite element model. Therefore, in order to simplify the FE model, the CT scan data was largely classified into exocuticle and endocuticle using VGSTUDIO MAX and then outputted as STL data. The .stl file was post-processed using HyperMesh ver.2022.1 (Altair Engineering, Inc., Tokyo, Japan) to generate meshes suitable for FEA. At that time, small protrusions on the surface were removed, and internal pores and pct ⊥ surface were changed to exocuticle for the surface layer and endocuticle for the interior. The thickness of the exocuticle, which corresponds to the surface layer of the claw that is strongly affected by the pinching force, was kept constant at 0.3 mm. The FE mesh for the exocuticle area was divided into four elements in the thickness direction, i.e., the mesh size in the thickness direction is constant, 0.075 mm. The hexahedral element was used for the exocuticle

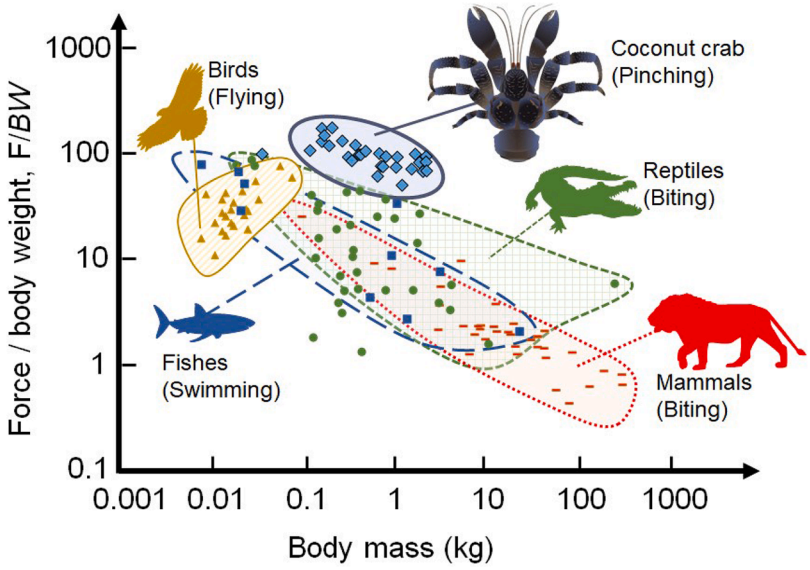

Fig. 1. The maximum force per unit body mass vs. body mass of several animal groups, including coconut crabs.

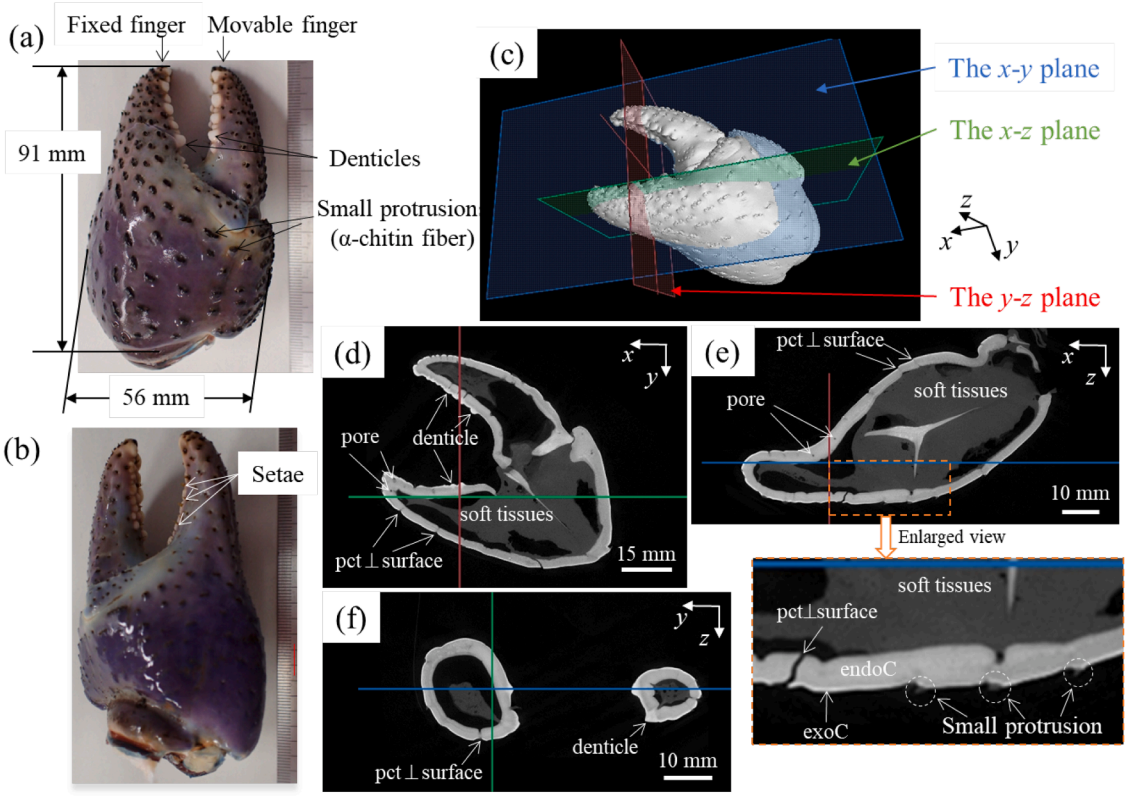

Fig. 2. (a) Top and (b) bottom of the left claw of the coconut crab. (c) Tomographic reconstruction of its claw; ortho-slice views of (d) the *x*–*y* plane, (e) the *x*–*z* plane, and (f) the *y*–*z* plane shown in (c). The X-ray CT images shown in (d–f) show that the calcium concentration increases as the color becomes whiter. Here, pct denotes pore canal tubules, exoC denotes endocuticle, and endoC denotes endocuticle.

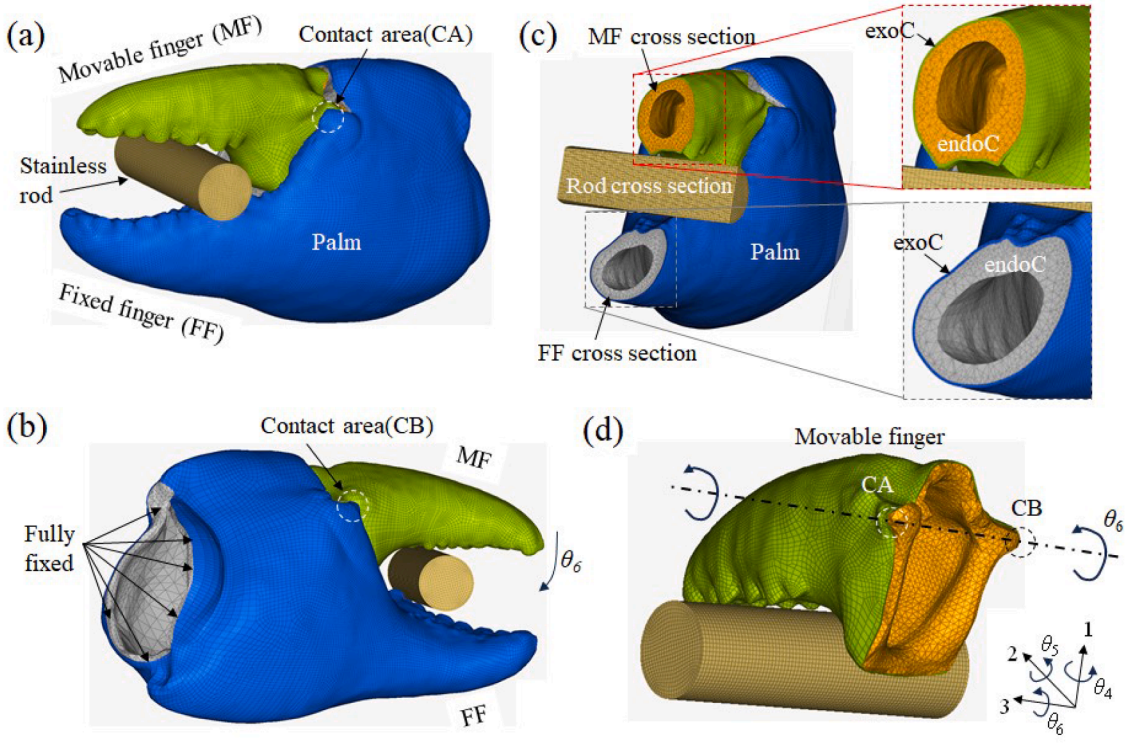

Fig. 3. Initial conditions of the finite element model in the claw; (a) top, (b) bottom, (c) cross section, and (d) rotation axis defined in the contact area between the movable finger and the claw palm and the direction of rotation.

and the tetrahedral element was used for the endocuticle. First, a model of the entire claw using AutoMesh (element type: tetrahedral elements) was created and FEA was performed. However, there was a problem with low stress in the contact area and the stress distribution not being smooth, so we changed only the 0.3 mm part on the outer surface to hexahedral elements. The mesh in the exocuticle included 162,620 nodes and 129,100 elements, and the mesh in the endocuticle included 70,500 nodes and 287,923 elements. The Young's modulus was determined based on the nanoindentation results: 60 GPa for the exocuticle and 18 GPa for the endocuticle [15]. A Poisson ratio of 0.3 was used for both.

2.4. Finite element simulation

A 3D static FEA was applied using an explicit FE code Radioss ver. 2022.1 (Altair Engineering, Inc., Tokyo, Japan). In a pinching experiment [10], the force exerted by the crab while pinching a stainless steel stick-shaped sensor was measured. Similarly, a simulation was performed in which a stainless steel rod was pinched by the crab claw, as shown in Fig. 3(a). The rod diameter of 11.5 mm measured using calipers and the material data (Young's modulus of 210 GPa, Poisson's ratio of 0.3, and yield stress of 2000 GPa) of general martensitic stainless steel were used in the FEA. The hexahedral element was used for the bar, and the mesh included 52,569 nodes and 48,960 elements. As shown in Fig. 3(b), the end of the claw was completely fixed. The claw was divided into hard exocuticle (0.3 mm thick) and soft endocuticle, as shown in Fig. 3(c). The rod was placed on the fixed finger and left free. An axis passing through the contact area (CA and CB) between the movable finger and the claw palm was defined, as shown in Fig. 3(d), and a pinching simulation was performed in which the movable fingers rotated in the θ_6 direction to pinch the rod. All directions (1, 2, 3, θ_4, θ_5) other than the rotation direction θ_6 on this axis were fixed. The pinching force (R_f) was calculated as the sum of the node reaction forces in the area that came into contact with the rod during the rotation. A Coulomb condition, with a friction coefficient (μ) in a range between 0.1 and 0.5, was used as the friction condition between the claw and the rod. The FE results were outputted using HyperView ver.2022.1 (Altair Engineering, Inc., Tokyo, Japan).

3. Results and discussion

3.1. Validity of analysis conditions

Fig. 4 shows the relationship between the reaction force (= the pinching force R_f) and the rotation angle of the movable finger, θ_6, against the friction coefficient, μ, during pinching. It also shows contour maps of the nodal reaction force. The R_f of the movable finger side was slightly larger than that of the fixed finger side; however, when $\mu = 0.5$, they were almost the same. This means that, although the 3D shapes of the fingers of a crab claw are not the same on the fixed side as on the movable side, the forces are balanced during pinching. In other words, the rod is stably pinched, and the present analytical conditions are reasonable. The R_f increases with increasing θ_6; however, when the μ is 0.1 or 0.3, the R_f peaks at θ_6=0.3–0.5°, then decreases and increases again. This is thought to be the effect of slip in the contact area between the rod and the claw fingers. After the rod is completely stuck between the two fingers, the R_f increases significantly and linearly with θ_6, reaching 957 N at $\theta_6 \approx 2.8°$ regardless of μ.

3.2. Magnitude of von Mises stress during pinching

Fig. 5 shows contour maps of the von Mises stress, σ_{mises}, on the cross section in the contact areas between the rod and fingers under $\mu = 0.3$ and of σ_{mises} on the movable and fixed fingers at θ_6 =0.4°, 1.62°, 1.93°, and 2.8° Here, the values displayed on the rod, movable finger, and fixed finger are the maximum Mises stress, $\sigma_{mises(max)}$, in each region. When θ_6 is 0.4°, the σ_{mises} occurs in one area on the movable finger side (called area A) and one area on the fixed finger side. When $\theta_6 = 1.62$, it can be seen that the σ_{mises} occurs in one additional area on the movable finger side (called area B), i.e., $\sigma_{mises(max)} = 67$ MPa in area A and $\sigma_{mises(max)} =$ 52 MPa in area B. When $\theta_6 = 1.93°$, where the R_f begins to increase significantly, as shown in Fig. 4(b), the stress in area A disappears, the σ_{mises} in area B increases to 288 MPa, and $\sigma_{mises} = 18$ MPa occurs in a new area (called area C). At the final angle of 2.8°, the $\sigma_{mises(max)}$ in area C is 588 MPa, and the $\sigma_{mises(max)}$ in area B is 361 MPa. On the fixed finger side, the stress occurs in only one area regardless of the θ_6. As the θ_6 increases, the region where stress occurs becomes wider, and the $\sigma_{mises(max)}$ increases with θ_6 after the rod is completely stuck between the two fingers. At θ_6 =2.8°, an extremely large stress of 1777 MPa occurs. The areas where stress occurs in these claw fingers are the denticles on the pinching side. In the coconut crab's claws, relatively large denticles are arranged in a line on the top side, and small denticles are randomly arranged on the inside [16,26]. The presence of these denticles allows the omnivorous coconut crab to capture prey of various shapes and hardness, and it does not let go easily once it has pinched something. In this analysis, the rod was unstable until there was a small rotation angle (~1.62°); however, when the R_f began to increase to θ_6 =1.93, it became stable by being sandwiched between two denticles on the movable finger and one denticle on the fixed finger, and the stress generated in these denticles increased with θ_6. The $\sigma_{mises(max)}$ generated in the surface layer of the rod in contact with the fixed denticle was 110 MPa for θ_6 =0.4°, 170 MPa for θ_6 =1.62°, 413 MPa for θ_6 =1.93°, and 674 MPa for

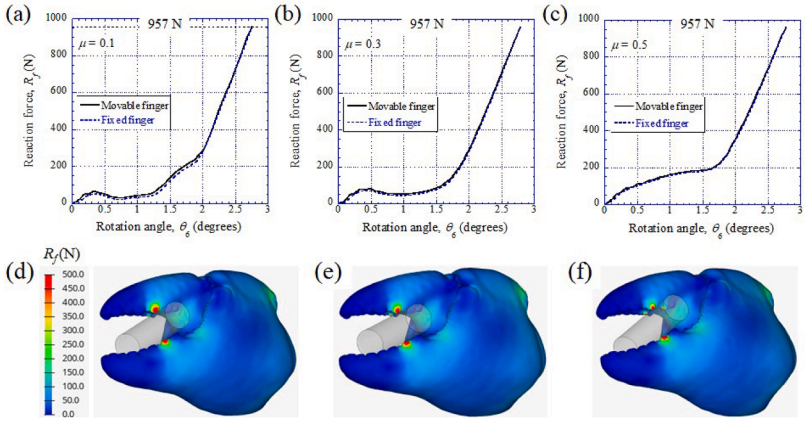

Fig. 4. Reaction force R_f – rotation angle θ_6 curves against the friction coefficient, μ, of (a) 0.1, (b) 0.3, and (c) 0.5 on the movable finger side and the fixed finger side. Contour maps of the nodal reaction force at $\theta_6 \approx 2.8°$ under μ of (d) 0.1, (e) 0.3, and (f) 0.5.

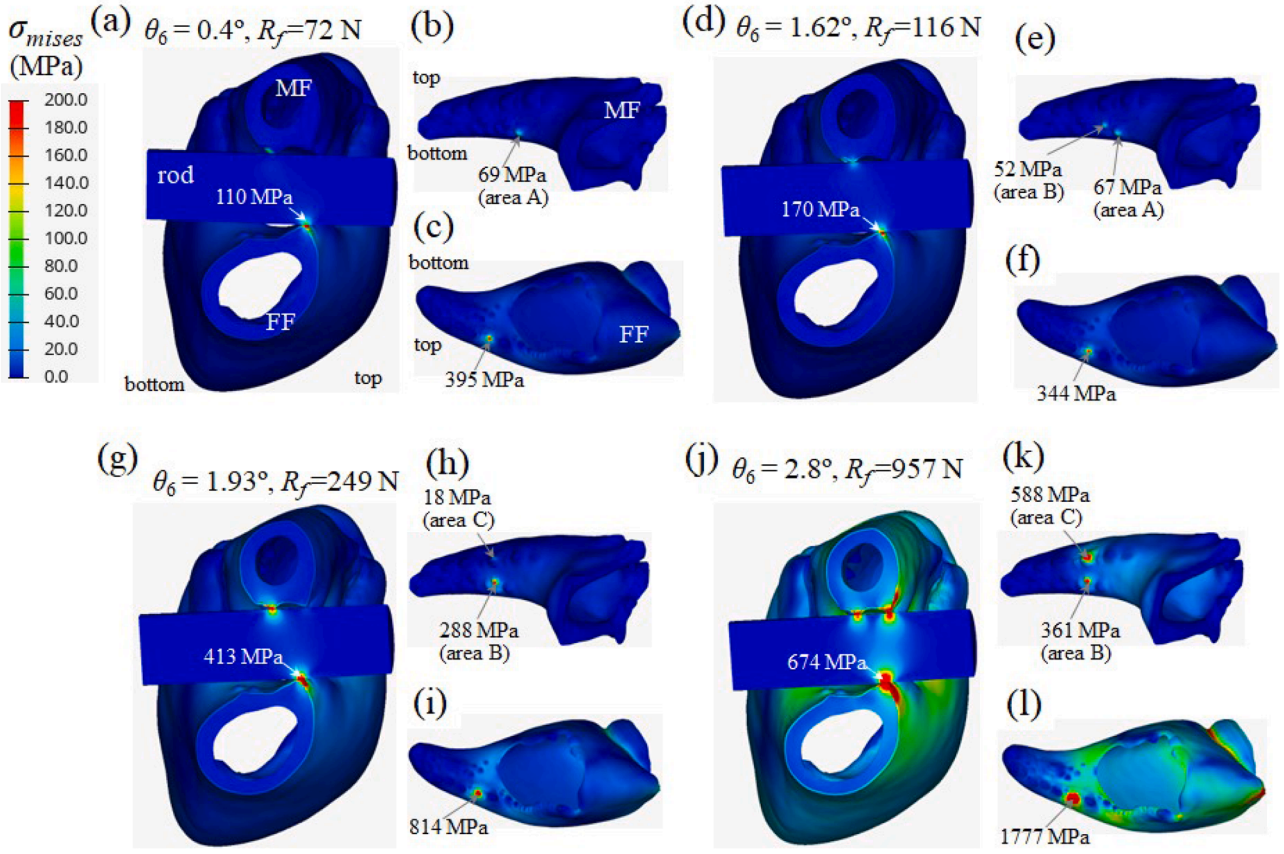

Fig. 5. Contour maps of von Mises stress, σ_{mises}, of (a,d,g,j) the cross section, (b,e,h,k) movable finger (MF), and (c,f,i,l) fixed finger (FF) with θ_6, under $\mu = 0.3$: (a–c) θ_6 =0.4°, (d–f) θ_6 =1.62°, (g–i) θ_6 =1.93°, and (j-l) θ_6 =2.8° Here, R_f denotes a reaction force of the movable finger side.

θ_6 =1.62. These magnitudes were below the yield stress of the stainless steel rod.

The maximum stress in the denticles on the claw fingers was located internally, rather than on the surface. Fig. 6 shows contour maps of σ_{mises} on the cross section in the area where $\sigma_{mises(max)}$ occurs on the fixed finger side, which corresponds to Fig. 5(l), including the FE mesh. The location of $\sigma_{mises(max)}$=1.8 GPa was the center of the 0.3 mm thickness of the exocuticle at the surface layer, and the σ_{mises} rapidly decreased within the endocuticle. Based on the well-known Hertzian solutions [27], it is reasonable that the maximum stress occurs inside the contacting area, and it is natural that the stress decreases in the soft endocuticle. The pinching simulation revealed that the maximum stress generated inside the exocuticle was 1.8 GPa. In contract, the maximum stress generated inside the endocuticle was 690 MPa. The pinching side of the claw finger has many denticles, and the exoskeleton has a soft endocuticle, which helps distribute the force during pinching. The size, shape, and arrangement of the denticles on the pinching side of the crab claw vary from crab to crab. In the case of coconut crabs, the pinching side of the claw has many large and small denticles arranged irregularly [26]. The front side of the claw has a row of relatively large denticles,

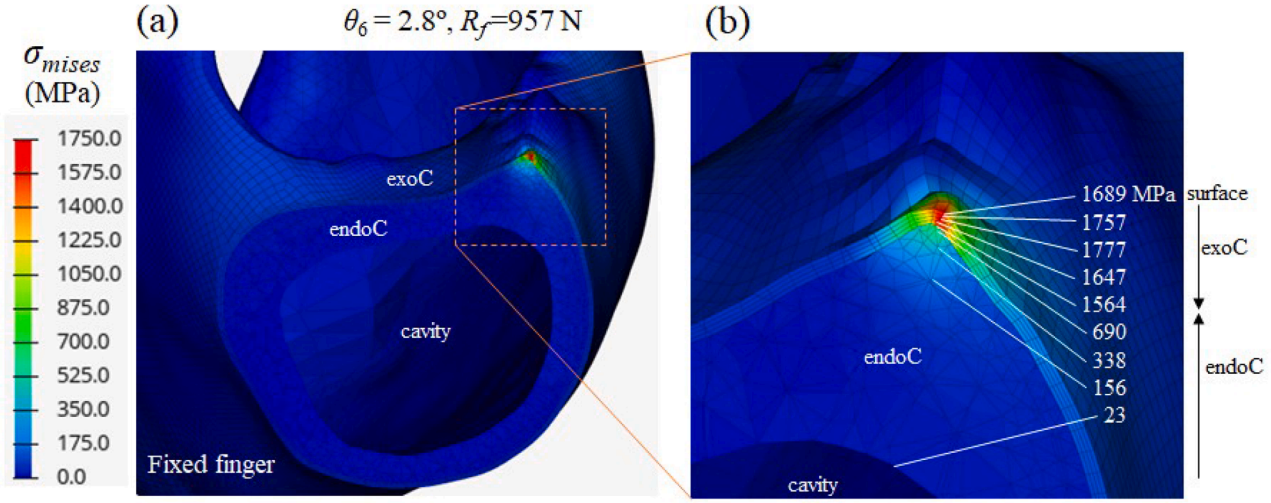

Fig. 6. (a) Contour map of σ_{mises} of fixed finger cross section under $\mu = 0.3$ and (b) enlarged view. Here, the values in (b) denote a magnitude of σ_{mises} at each node.

while the back side has small denticles arranged randomly. The function of the claw (pinching, crushing, cutting) varies depending on the crab species and habitat. The pinching simulation presented in this study will help elucidate the functions of various crab claws.

Strictly speaking, the coconut crab's exoskeleton is a functionally graded material, with hardness and Young's modulus gradually decreasing from the surface [15,16], and it consists of mineralized and non-mineralized regions [22]. The gel-like substance in the indirect area is very soft, so it may have the effect of reducing the pinching force. In addition, a coconut crab pinches prey at high strain rates, and the pinched state is maintained. Therefore, the effect of speed must be taken into account; mechanical properties that depend on the strain rate are required for the exoC, endoC, and denticles that make up the exoskeleton. In order to get closer to reality and improve the accuracy of the analysis, pinching simulations that account for these effects will be necessary in the future. We believe that such simulations can be used to develop designs for the 3D geometry and internal structure needed to create tips of robot arms [28] that never let go once they have pinched or tips of medical forceps that are not easily broken.

4. Conclusion

A pinching simulation was performed that took into account the three-dimensional shape of the coconut crab claw, as well as its internal hard and soft layers. This was achieved through the use of microfocus X-ray computed tomography, image analysis software and finite element analysis. When a coconut crab pinched a stainless steel rod, the Mises stress generated at the contact surface of the claw fingers was quantified. The pinching force and stress increased with the rotation angle of the movable finger, regardless of the friction coefficient of the contact area between the rod and the claw fingers. The results showed that maximum stresses of 1.8 GPa in the fixed finger, 588 MPa in the movable finger, and 674 MPa in the stainless rod were generated. This analysis scientifically confirms the exceptional strength of the coconut crab's claw.

CRediT authorship contribution statement

Tadanobu Inoue: Writing – review & editing, Writing – original draft, Visualization, Validation, Supervision, Resources, Project administration, Methodology, Investigation, Funding acquisition, Data curation, Conceptualization. **Michinori Iwai:** Writing – review & editing, Visualization, Software, Methodology, Investigation, Formal analysis, Data curation.

Declaration of competing interest

The authors declare that they have no known competing financial interests or personal relationships that could have appeared to influence the work reported in this paper.

Acknowledgements

S. Oka (Okinawa Churashima Foundation) provided valuable ecological insights on coconut crabs and showed us the equipment used for the pinching experiment. This study was supported by JSPS KAKENHI Grant Number JP21H04537, Japan; and Iketani Science and Technology Foundation Grant Number 0361243-A, Japan. The grants are greatly appreciated.

Data availability

No data was used for the research described in the article.

References

[1] A. Garg, A. Sharma, W. Zheng, L. Li, Dactyl club and nacre-inspired impact resistant behavior of layered structures: a review of present trends and prospects, Mater. Today Commun. 28 (2024) 110553, https://doi.org/10.1016/j.mtcomm.2024.110553.
[2] M. Vittori, Structural diversity of crustacean exoskeletons and its implications for biomimetics, Interface Focus 14 (2024) 20230075, https://doi.org/10.1098/rsfs.2023.0075.
[3] L. Bai, L. Liu, M. Esquivel, B.L. Tardy, S.;. Huan, X.;. Niu, S.;. Liu, G. Yang, Y. Fan, O.J. Rojas, Nanochitin: chemistry, structure, assembly, and applications, Chem. Rev. 122 (2022) 11604–11674, https://doi.org/10.1021/acs.chemrev.2c00125.
[4] H. Yao, G. Zheng, W. Li, M.T. McDowell, Z. Seh, N. Liu, Z. Lu, Y. Cui, Crab shells as sustainable templates from nature for nanostructured battery electrodes, Nano Lett. 13 (2013) 3385–3390, https://doi.org/10.1021/nl401729r.
[5] B. Zhang, Q. Han, J. Zhang, Z. Han, S. Niu, L. Ren, Advanced bio-inspired structural materials: local properties determine overall performance, Mater. Today 41 (2020) 177–199, https://doi.org/10.1016/j.mattod.2020.04.009.
[6] B. Bhushan, Biomimetics: lessons from nature – an overview, Phil. Trans. R. Soc. A. 367 (2009) 1445–1486, https://doi.org/10.1098/rsta.2009.0011.
[7] R.M. Alexander, The maximum forces exerted by animals, J Experimental Biol 115 (1985) 231–238. https://jeb.biologists.org/content/jexbio/115/1/231.full.pdf.
[8] G.M. Taylor, Maximum force production: why are crabs so strong? Proc. Biol. Sci. 267 (2000) 1475–1480, https://doi.org/10.1098/rspb.2000.1167.
[9] D.R. Huber, T.G. Eason, R.E. Hueter, P.J. Motta, Analysis of the bite force and mechanical design of the feeding mechanism of the durophagous horn shark Heterodontus francisci, J. Experimental Biol. 208 (2005) 3553–3571, https://doi.org/10.1242/jeb.01816.
[10] S. Oka, T. Tomita, K. Miyamoto, A mighty claw: pinching force of the coconut crab, the largest terrestrial crustacean, PLOS ONE 11 (2016) e0166108, https://doi.org/10.1371/journal.pone.0166108.
[11] Y. Bouligand, Twisted fibrous arrangements in biological materials and cholesteric mesophases, Tissue and Cell 4 (1972) 189–217, https://doi.org/10.1016/S0040-8166(72)80042-9.
[12] H.O. Fabritius, E.S. Karsten, K. Balasundaram, S. Hild, K. Huemer, D. Raabe, Correlation of structure, composition and local mechanical properties in the dorsal carapace of the edible crab Cancer pagurus, Z. Kristallogr. 227 (2012) 766–776, https://doi.org/10.1524/zkri.2012.1532.
[13] F. Zhou, Z. Wu, M. Wang, K. Chen, Structure and mechanical properties of pincers of lobster (Procambarus clarkii) and crab (Eriocheir Sinensis), J. Mech. Behav. Biomed. Mater. 3 (2010) 454–463, https://doi.org/10.1016/j.jmbbm.2010.05.001.
[14] T. Inoue, S. Oka, T. Hara, Three-dimensional microstructure of robust claw of coconut crab, one of the largest terrestrial crustaceans, Mater. Design. 206 (2021) 109765, https://doi.org/10.1016/j.matdes.2021.109765.
[15] T. Inoue, T. Hara, K. Nakazato, S. Oka, Superior mechanical resistance in the exoskeleton of the coconut crab, *Birgus latro*, Mater. Today Bio 12 (2021) 100132, https://doi.org/10.1016/j.mtbio.2021.100132.
[16] T. Inoue, S. Oka, K. Nakazato, T. Hara, Structural changes and mechanical resistance of claws and denticles in coconut crabs of different sizes, Biology (Basel) 10 (2021) 1304, https://doi.org/10.3390/biology10121304.
[17] Y. Ma, C. Guo, N. Dai, J. Shen, J. Guan, Structural characterization and regulation of the mechanical properties of the carapace cuticle in tri-spine horseshoe crab (Tachypleus tridentatus), J. Mech. Behav. Biomed. Mater. 125 (2022) 104954, https://doi.org/10.1016/j.jmbbm.2021.104954.
[18] Z.L. Zhao, T. Shu, X.Q. Feng, Study of biomechanical, anatomical, and physiological properties of scorpion stingers for developing biomimetic materials, Mater Sci Eng. C. 58 (2016) 1112–1121, https://doi.org/10.1016/j.msec.2015.09.082.
[19] M. Vittori, V. Srot, L. Korat, M. Rejec, P. Sedmak, B. Bussmann, F. Predel, P. A. Aken, J. Štrus, The mechanical consequences of the interplay of mineral distribution and organic matrix orientation in the claws of the sea slater Ligia pallasii, Minerals 11 (2021) 1373, https://doi.org/10.3390/min11121373.
[20] T. Inoue, E. Kitahara, Y. Hara, K. Nakazato, Mud crab's mottled, deep-blue exoskeleton: surface morphology and internal microstructure, Minerals 12 (2022) 1607, https://doi.org/10.3390/min12121607.
[21] Z. Qian, M. Yang, L. Zhou, J. Liu, R. Akhtar, C. Liu, Y. Liu, L. Ren, L. Ren, Structure, mechanical properties and surface morphology of the snapping shrimp claw, J Mater. Sci. 53 (2018) 10666–10678, https://doi.org/10.1007/s10853-018-2364-7.
[22] T. Inoue, S. Oka, T. Hiroto, Mechanical properties, tissue structure, and elemental composition of the walking leg tips of coconut crabs, J. Marine Sci. Eng. 12 (2024) 639, https://doi.org/10.3390/jmse12040639.
[23] Y. Yang, S. Qin, C. Di, J. Qin, D. Wu, J. Zhao, Research on claw motion characteristics and cavitation bubbles of snapping shrimp, Appl. Bionics Biomech. 2020 (2020) 6585729, https://doi.org/10.1155/2020/6585729.
[24] P.R. Sayekti, Cerniauskas G Fahrunnida, C. Robert, B. Retnoaji, P. Alam, The impact behaviour of crab carapaces in relation to morphology, Materials (Basel) 13 (2020) 3994, https://doi.org/10.3390/ma13183994.
[25] S. Oka, K. Miyamoto, S. Matsuzaki, T. Sato, Growth of the coconut crab, *Birgus latro*, at its northernmost range estimated from Mark–Recapture using individual identification based on carapace grooving patterns, Zool. Sci. 32 (2015) 260–265, https://doi.org/10.2108/zs150008.

[26] T. Inoue, S. Oka, K. Nakazato, T. Hara, Columnar structure of claw denticles in the coconut crab, *Birgus latro*, Minerals 12 (2022) 274, https://doi.org/10.3390/min12020274.
[27] F.W. Zok, A. Miserez, Property maps for abrasion resistance of materials, Acta mater 55 (2007) 6365–6371, https://doi.org/10.1016/j.actamat.2007.07.042.
[28] J. Kwon, D. Bombara, C. Teeple, J. Lee, C. Hoberman, R. Wood, J. Werfel, Transformable linkage-based gripper for multi-mode grasping and manipulation, IEEE Robotics and Automation Letters 8 (2023) 8446–8453, https://doi.org/10.1109/LRA.2023.3329758.